

Tomonaga–Luttinger parameters and spin excitations in the dimerized extended Hubbard model

Satoshi Ejima¹, Florian Gebhard¹, and Satoshi Nishimoto²

¹*Fachbereich Physik, Philipps-Universität Marburg, D-35032 Marburg, Germany*

²*Max-Planck-Institut für Physik komplexer Systeme, D-01187 Dresden, Germany*

(Dated: July 6, 2021)

We study the one-dimensional extended Hubbard model with alternating size of the hopping integrals using the density-matrix renormalization group method. We calculate the spin gap, the Tomonaga–Luttinger parameter, and the charge-density-wave order parameter for various dimerizations, interaction strengths, and band fillings. At half band-filling the spin and charge excitations are gapped but these gaps disappear for infinitesimal hole doping. At quarter filling, the Umklapp scattering in the half-filled lower Peierls band generates a gap for the charge excitations but the gapless spin excitations can be described in terms of an effective antiferromagnetic Heisenberg model. Beyond a critical strength for the nearest-neighbor interaction, the dimerized extended Hubbard model at quarter filling develops a charge-density-wave ground state. The dimerization and the nearest-neighbor Coulomb interaction strongly reduce the Tomonaga–Luttinger parameter from its value for the bare Hubbard model. We discuss the relevance of our findings for the Bechgaard salts.

PACS numbers: 71.10.Pm, 71.10.Fd, 78.30.Jw, 72.15.Nj

I. INTRODUCTION

The Bechgaard salts are organic conductors which have attracted much interest over the last thirty years^{1,2}. Upon variation of the pressure, the temperature, and the anion X in $(\text{TMTSF})_2X$ and $(\text{TMTTF})_2X$, these compounds exhibit a rich phase diagram, e.g., a superconducting phase is found to lie in-between a paramagnetic metallic phase and a spin-density-wave phase. The systems can be regarded as quasi one-dimensional due to the strong anisotropy of the transport along the three crystalline axes. Recent experiments³ support the view that the metallic phase can be characterized as a Tomonaga–Luttinger liquid at temperatures $T > 100$ K. Indeed, signatures of the Tomonaga–Luttinger liquid are the reduced density of states at the Fermi energy as seen in angle-resolved photoemission spectroscopy^{4,5}, the negative temperature dependence of the c-axis resistivity⁶, the scaling behavior of high-energy range of the optical conductivity⁷, the power-law temperature dependence of the Hall coefficient^{8,9}, and the empirical relationship $(T_1 T)^{-1} \propto \chi_s^2(T)$ between the measured spin relaxation rate and the magnetic susceptibility in nuclear magnetic resonance measurements^{10,11}. Moreover, distinctly different thermal conductivities for the charge and spin excitations have been reported which provide evidence for spin-charge separation¹².

All correlation functions in the Tomonaga–Luttinger liquid display a power-law behavior with unusual, interaction-dependent coefficients. Many of them are simple functions of the so-called Tomonaga–Luttinger parameter K_ρ . Most experiments give $K_\rho \approx 0.2$ for the Bechgaard salts. The single-band Hubbard model in which spin-1/2 electrons move on a chain and interact only locally is one of the best studied Hamiltonians for correlated lattice electrons. However, the model gives $K_\rho \geq 0.5$ for all interaction strengths which shows that

the long-range parts of the Coulomb interaction must be taken into account for a proper description of the Bechgaard salts. In the extended Hubbard model the long-range parts of the Coulomb interaction are mimicked by a nearest-neighbor term^{13,14,15}.

Other factors may also play an important role. For instance, the stacks of TMTTF and TMTSF molecules form dimerized chains and the alternation of the electron transfer-matrix elements along the chain must be considered. Therefore, in this work we study the one-dimensional extended Hubbard model with alternating hopping amplitudes, i.e., the one-dimensional dimerized extended Hubbard model as the minimal one-dimensional, purely electronic model for the electronic excitations in the Bechgaard salts. The relevant bands in the TMTSF and TMTTF salts are filled with three electrons so that the system is quarter-filled in hole notation, and we use the hole picture in the following.

There are few systematic studies of the dimerized extended Hubbard model in the literature. Therefore, we investigate the model for various band fillings, with an emphasis on the vicinity of the commensurate fillings. In this way, our principle investigation of correlated electrons in quasi one-dimensional dimerized systems could be relevant also for other materials, e.g., for the inorganic spin-Peierls system CuGeO_3 ¹⁶.

In our work we apply the density-matrix renormalization group (DMRG) method which is one of the most reliable numerical methods to study the low-energy properties of one-dimensional correlated electron systems. Where applicable, we compare our results to the predictions from field theory and effective single-band Hubbard models.

Our paper is organized as follows. In Sec. II we define the dimerized extended Hubbard model and introduce the physical quantities of interest, namely, the spin gap, the charge-density-wave (CDW) order parameter,

and the Tomonaga–Luttinger parameter. In Sec. III, we separately present our DMRG results for the dimerized Hubbard model with and without the nearest-neighbor interaction, and discuss the experimental relevance of our investigations. We close with a short summary in Sect. IV.

II. MODEL AND METHOD

A. Hamiltonian

In order to model the Bechgaard salts, we focus on the transport of a chain of stacked molecules and regard a single TMTTF or TMTSF molecule as a site. The chain has a geometrical (Peierls) modulation. Besides the intra-molecular Coulomb interaction, we should take into account a nearest-neighbor Coulomb repulsion because of the fairly short inter-molecular distance. Thus, our model Hamiltonian of choice is the one-dimensional dimerized extended Hubbard model for spin-1/2 electrons on L lattice sites

$$\hat{H} = -t_1 \sum_{l,\text{odd}} (\hat{c}_{l+1\sigma}^\dagger \hat{c}_{l\sigma} + \text{h.c.}) - t_2 \sum_{l,\text{even}} (\hat{c}_{l+1\sigma}^\dagger \hat{c}_{l\sigma} + \text{h.c.}) + U \sum_l \hat{n}_{l\uparrow} \hat{n}_{l\downarrow} + V \sum_l (\hat{n}_l - n)(\hat{n}_{l+1} - n), \quad (1)$$

where $\hat{c}_{l\sigma}^\dagger$ ($\hat{c}_{l\sigma}$) is the creation (annihilation) operator of an electron with spin $\sigma = \uparrow, \downarrow$ at site l , $\hat{n}_{l\sigma} = \hat{c}_{l\sigma}^\dagger \hat{c}_{l\sigma}$ is the number operator, and $\hat{n}_l = \hat{n}_{l\uparrow} + \hat{n}_{l\downarrow}$. The total number of electrons is $N = N_\uparrow + N_\downarrow$, and $n = N/L$ is the average number of electrons per lattice site. The electron transfer matrix elements t_1 and $t_2 < t_1$ model the dimerization of the chain, U is the strength of the Hubbard interaction, and V parametrizes the nearest-neighbor Coulomb repulsion. We call a pair of sites which is connected by the hoping amplitude t_1 a ‘dimer’.

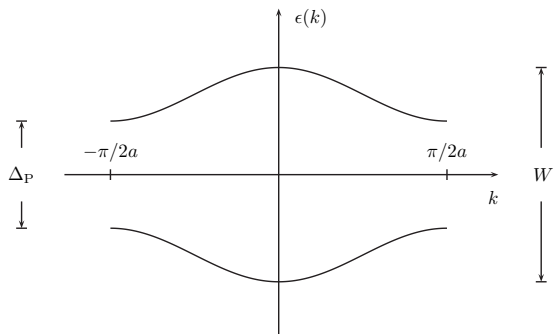


FIG. 1: Band structure for non-interacting electrons in a dimerized chain.

The dimerization splits the tight-binding cosine band into a bonding band (‘lower Peierls band’) and an anti-bonding band (‘upper Peierls band’). The bare band

structure is shown in Fig. 1. The dispersion relation of the two Peierls bands is given by

$$\epsilon_{1,2}(k) = \pm \sqrt{t_1^2 + t_2^2 + 2t_1 t_2 \cos k} \quad \text{for } |k| \leq \frac{\pi}{2a}, \quad (2)$$

where a is the lattice spacing which we set to unity in the following. The gap between the two Peierls bands is $\Delta_P = 2(t_1 - t_2)$. The total band width is $W = 2(t_1 + t_2)$. In the absence of a dimerization, for $t_1 = t_2 = t$, we recover the band structure of the tight-binding model in the reduced zone scheme.

B. Physical quantities

In this work we employ the DMRG method which provides very accurate data for ground-state properties of one-dimensional correlated electron systems; for a review, see [17,18]. We use the DMRG to calculate the spin gap Δ_s , the CDW order parameter χ , and the Tomonaga–Luttinger parameter K_ρ . To this end, we consider a chain with $L/2$ dimers with $L/2$ even for a two-band system. We study chains with up to 320 sites and open-end boundary conditions. We keep up to $m = 3600$ density-matrix eigenstates in the DMRG procedure and extrapolate the calculated quantities to the limit $m \rightarrow \infty$. In this way, the maximum error in the ground-state energy is below $10^{-6}t_1$. Lastly, we extrapolate our finite-size results to the thermodynamic limit, $L \rightarrow \infty$.

The spin gap is defined by

$$\Delta_s = \lim_{L \rightarrow \infty} \Delta_s(L),$$

$$\Delta_s(L) = E_0(L, N_\uparrow + 1, N_\downarrow - 1) - E_0(L, N_\uparrow, N_\downarrow), \quad (3)$$

where $E_0(L, N_\uparrow, N_\downarrow)$ is the ground state energy of a system of length L with N_\uparrow up-spin and N_\downarrow down-spin electrons.

Later in this work, we shall focus on the CDW ground state of our model (1) at quarter band filling. For large enough nearest-neighbor repulsion V we expect a CDW with a wave vector $Q_{\text{CDW}} = 4k_F$. Here, $k_F = \pi n/2$ is the Fermi wave number. At quarter band filling, $n = 1/2$, we have $k_F = \pi/4$ which corresponds to a half-filled lower Peierls band.

The order parameter for the $4k_F$ -CDW phase is defined by

$$\chi = \lim_{L \rightarrow \infty} \chi(L), \quad (4)$$

$$\chi(L) = \left| \frac{1}{r+2} \sum_{l=(L-r)/2}^{(L+r)/2+1} (-1)^l \langle \hat{n}_l \rangle \right|. \quad (5)$$

In (5) the summation over the lattice sites l is restricted to a region r around the central site of the chain in order to reduce the edge effects. We set $r = 2$ for a systematic extrapolation to the thermodynamic limit. Of course,

the extrapolated results should be independent of the choice of the range r . On finite lattices and for open-end boundary conditions, the Friedel oscillations from the edges result in a finite value for $\chi(L)$, and a well-controlled finite-size extrapolation is mandatory.

For the calculation of the Tomonaga–Luttinger parameter K_ρ we use a new method which we proposed recently¹⁹. The Tomonaga–Luttinger parameter K_ρ determines the long-range decay of the density-density correlation function in the metallic Tomonaga–Luttinger liquid ground state. It is defined by the ground-state expectation value

$$C^{\text{NN}}(r) = \frac{1}{L} \sum_{l=1}^L \langle \hat{n}_{l+r} \hat{n}_l \rangle - \langle \hat{n}_{l+r} \rangle \langle \hat{n}_l \rangle. \quad (6)$$

Using conformal field theory it can be shown^{20,21} that the asymptotic behavior for $1 \ll r \ll L$ is given by

$$C^{\text{NN}}(r) \sim -\frac{K_\rho}{(\pi r)^2} + \frac{A \cos(2k_F r)}{r^{1+K_\rho}} \ln^{-3/2}(r) + \dots, \quad (7)$$

where A is a constant. In previous approaches^{22,23,24,25}, K_ρ was extracted from the Fourier transformation of $C^{\text{NN}}(r)$ but in a real-space DMRG approach the accuracy of the correlation function becomes increasingly worse as the distance r increases. In Ref. [19] we calculated the density-density correlation function directly in Fourier space. We address

$$N(q) = \frac{2}{L} \langle \hat{n}(q) \hat{n}(-q) \rangle, \quad (8)$$

where $\hat{n}(q)$ is given by

$$n(q) = \sum_{l,\text{odd}} e^{i(q/2)(l+1/2-r_c)} (\hat{c}_{l\sigma}^\dagger \hat{c}_{l\sigma} + \hat{c}_{l+1\sigma}^\dagger \hat{c}_{l+1\sigma}). \quad (9)$$

Here, $r_c = (L+1)/2$ denotes the central position of the chain. The derivative of $N(q)$ at $q=0$ directly gives the Tomonaga–Luttinger parameter. In practice, we obtain it from

$$\begin{aligned} K_\rho &= \lim_{L \rightarrow \infty} K_\rho(L), \\ K_\rho(L) &= \frac{L}{4} N\left(\frac{4\pi}{L}\right). \end{aligned} \quad (10)$$

For a precise calculation of K_ρ is important to target not only the ground state $|\Phi_0\rangle$ but also the state $|\Psi_q\rangle = \hat{n}(-q)|\Psi_0\rangle$ in the DMRG procedure; see Ref. [19] for further details.

The Tomonaga–Luttinger parameter is well defined only for the metallic Tomonaga–Luttinger liquid. Later we shall investigate K_ρ for insulators which are infinitesimally doped away from their commensurate doping n_c . In these cases we give

$$K_\rho(n \rightarrow n_c^\pm) = \lim_{L \rightarrow \infty} K_\rho \left(n = n_c \pm \frac{2}{L} \right). \quad (11)$$

This approach is very successful for the single-band Hubbard model, as demonstrated in Ref. [19].

C. Effective models

For not too small dimerizations, $t_2/t_1 \lesssim 0.9$, we can map the dimerized extended Hubbard model to an effective single-band extended Hubbard model¹³. The upper Peierls band can be integrated out and we are left with a Hubbard chain with $L/2$ dimer sites l_d with effective parameters,

$$\begin{aligned} \hat{H}_{\text{eff}} &= t_{\text{eff}} \sum_{l_d} (\hat{c}_{l_d+1\sigma}^\dagger \hat{c}_{l_d\sigma} + \text{h.c.}) + U_{\text{eff}} \sum_{l_d} \hat{n}_{l_d\uparrow} \hat{n}_{l_d\downarrow} \\ &\quad + V_{\text{eff}} \sum_{l_d} (\hat{n}_{l_d} - 1)(\hat{n}_{l_d+1} - 1), \end{aligned} \quad (12)$$

$$t_{\text{eff}} = \frac{t_2}{2}, \quad (13)$$

$$U_{\text{eff}} = 2t_1 - \frac{\sqrt{(U-V)^2 + 16t_1^2} - (U+V)}{2}, \quad (14)$$

$$V_{\text{eff}} = \frac{V}{4}. \quad (15)$$

The band filling is $n_{\text{eff}} = 2n$ so that $k_{F,\text{eff}} = \pi n$ and $v_{F,\text{eff}} = t_2 \sin(\pi n)$. Note that $U_{\text{eff}}/t_{\text{eff}}$ can be large even when U/t_1 is small, e.g., $U_{\text{eff}}/t_{\text{eff}} = 8.8$ for $U = t_1$, $V = 0$, and $t_2/t_1 = 0.1$.

For $V < V_c$ the quarter-filled dimerized extended Hubbard model describes a Mott–Hubbard insulator with gap-less spin excitations. In this parameter region, the spin degrees of freedom of the effective single-band Hubbard model (12) can be described by an effective Heisenberg model,

$$\hat{H}_{\text{heis,eff}} = J_{\text{eff}} \sum_{l_d} \hat{\mathbf{S}}_{l_d} \cdot \hat{\mathbf{S}}_{l_d+1}, \quad (16)$$

where $\hat{\mathbf{S}}_{l_d}$ is the spin operator for a dimer located at position l_d . Up to second-order in t_2/U_{eff} , we have

$$J_{\text{eff}}(V) = \frac{4t_2^2}{8t_1 + 2U + V - 2\sqrt{(U-V)^2 + 16t_1^2}}. \quad (17)$$

III. RESULTS

A. Dimerized Hubbard model

First, we consider the dimerized Hubbard model, i.e., we set $V = 0$ in (1).

1. Tomonaga–Luttinger parameter

In order to demonstrate the accuracy of our method, we address the Tomonaga–Luttinger parameter at small interactions, $U < W$, as a function of the dimerization in the metallic regime, $n = 0.4$. To lowest order in the

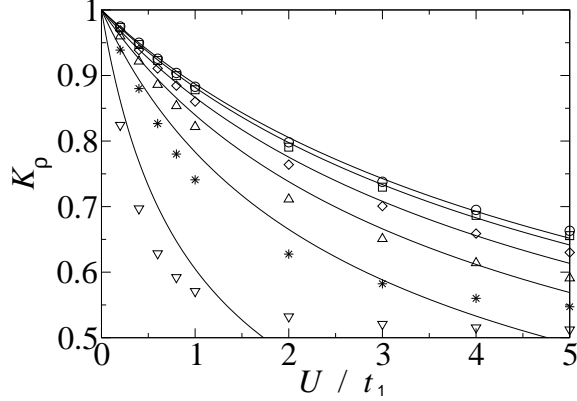


FIG. 2: Tomonaga–Luttinger parameter K_ρ from the DMRG approach (symbols) in comparison with the predictions from the g -ology method (solid lines), as a function of U/t_1 for $t_2/t_1 = 1, 0.9, 0.5, 0.3, 0.1$ (from top to bottom) at $n = 0.4$ for the dimerized Hubbard model.

couplings, $g_1 = g_2 = g_4 = U/2$, the field-theoretical ‘ g -ology’ approach predicts^{26,27}

$$K_\rho = \sqrt{\frac{2\pi v_F}{2\pi v_F + U}} \quad (18)$$

where the Fermi velocity v_F is given by

$$v_F = \frac{t_1 t_2 \sin k_F}{\sqrt{t_1^2 + t_2^2 + 2t_1 t_2 \cos(k_F)}}. \quad (19)$$

This result can be systematically improved with the functional Renormalization Group method²⁸.

In Fig. 2, we compare the Tomonaga–Luttinger parameter as calculated from the DMRG approach, eq. (10), to the g -ology prediction (18). We plot K_ρ as a function of U/t_1 for various dimerization strengths t_2/t_1 at band filling $n = 0.4$. The system is metallic for all interaction strengths. For all dimerizations, K_ρ decreases monotonically with increasing Coulomb interaction and finally approaches $K_\rho(U \rightarrow \infty) = 1/2$, as expected from the nondimerized Hubbard model. For small dimerization, $t_2/t_1 \gtrsim 0.5$, the DMRG results agree very well with those from the g -ology approach for all $U < W$. For small U/t_1 , K_ρ decreases weakly and monotonically with t_2/t_1 . This can be understood from the corresponding decrease of the bandwidth, $W = 2(t_1 + t_2)$, with a corresponding reduction of the Fermi velocity.

When the dimerization is large, $t_2/t_1 \lesssim 0.5$, and the Hubbard interaction is large, $U \gtrsim W/2$, the results from g -ology substantially deviate from the numerically exact DMRG results. The Tomonaga–Luttinger parameter K_ρ decreases rapidly with decreasing t_2/t_1 , and the g -ology predictions quickly violate the constraint $K_\rho \geq 1/2$. Apparently, higher-order corrections in U/W beyond the one-loop calculations needed to be considered.

As our next application, we investigate the Tomonaga–Luttinger parameter as a function of the band filling and the interaction strength. In Fig. 3, we show K_ρ from the

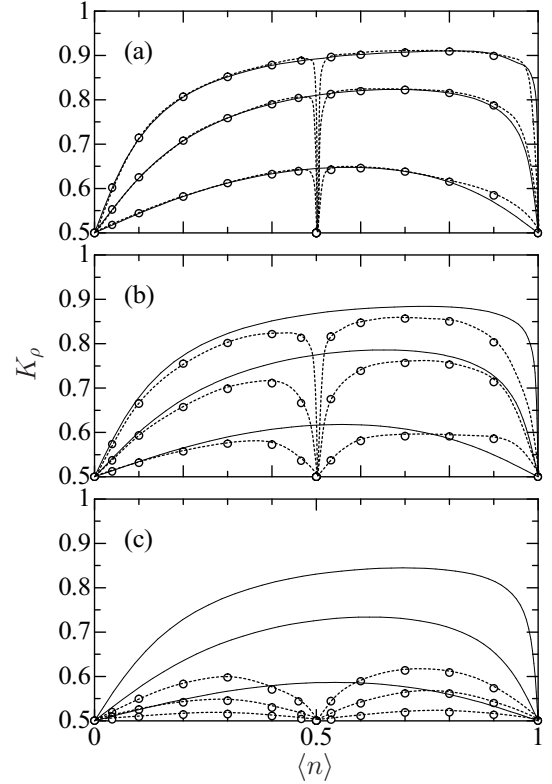


FIG. 3: Tomonaga–Luttinger parameter K_ρ as a function of the band-filling n for various dimerizations: (a) $t_2/t_1 = 0.9$, (b) $t_2/t_1 = 0.5$, and (c) $t_2/t_1 = 0.1$. In each figure, $U/t_1 = 1, 2, 6$ from top to bottom. Open circles denote the DMRG results in the dimerized Hubbard model, and dotted lines are guides for eyes. Solid lines give the exact result for the single-band Hubbard model with hopping integral $t = (t_1 + t_2)/2$.

DMRG method as a function of n for various interaction strengths U/t_1 and dimerizations: (a) $t_2/t_1 = 0.9$, (b) $t_2/t_1 = 0.5$, and (c) $t_2/t_1 = 0.1$. For comparison we also plot the exact results for K_ρ from the Bethe Ansatz for the one-dimensional single-band Hubbard model with the same band width, $t = (t_1 + t_2)/2$.

When the dimerization is small, $t_2/t_1 = 0.9$, we again find a good general agreement between the results for the dimerized Hubbard model and the single-band Hubbard model with the same total bandwidth. An exception is the narrow range around quarter band filling, $n = 1/2$. At quarter filling, the lower Peierls band is half filled and the Umklapp scattering becomes a (marginally) relevant perturbation which turns the metallic phase into a Mott–Hubbard insulator where K_ρ is not well defined, and we give the value for infinitesimal doping, see eq. (11). As expected from field theory^{27,29}, and confirmed numerically, we have

$$K_\rho \left(n = \frac{1}{2}^\pm \right) = \frac{1}{2} \quad (20)$$

for the density-driven Mott transition for all interaction strengths. This follows from the mapping of the quarter-

filled dimerized Hubbard model to the effective single-band Hubbard model at half band-filling. Therefore, K_ρ strongly changes as a function of density in the vicinity of quarter filling even for small dimerizations. The effect becomes more prominent with increasing dimerization strengths, see Fig. 3b.

When the dimerization is large, $t_2/t_1 = 0.1$, the single-band Hubbard model does not provide a good starting point for the analysis anymore. Instead, for large t_1/t_2 we rather consider the effective single-band Hubbard model (12) for $V = 0$. Because of the strong effective on-site interaction $U_{\text{eff}}/t_{\text{eff}}$, the Umklapp scattering strength becomes very large. For instance, the effective couplings at $t_2/t_1 = 0.1$ are estimated from eq. (14) as $U_{\text{eff}}/t_{\text{eff}} = 8.8, 15.3, 27.9$ for $V = 0$ and $U/t_1 = 1, 2, 6$, respectively. Therefore, the values for K_ρ are rather small for all $U/t_1 \gtrsim 1$. Moreover, the effective single-band Hubbard model always gives the correct result $K_\rho(n = 1/2^\pm) = 1/2$ because the quarter-filled dimerized Hubbard model maps onto the half-filled single-band Hubbard model which describes a Mott–Hubbard insulator for all interaction strengths.

As seen in Fig. 4, the quantitative agreement for K_ρ from the dimerized Hubbard model and the effective single-band Hubbard model is quite good for all U/t_1 at $t_2/t_1 = 0.1$. Note that the effective Hubbard model displays its particle-hole symmetry around $n = 1/2$ which the dimerized Hubbard model obeys only for $t_2/t_1 \rightarrow 0$ or $U/t_1 \rightarrow \infty$.

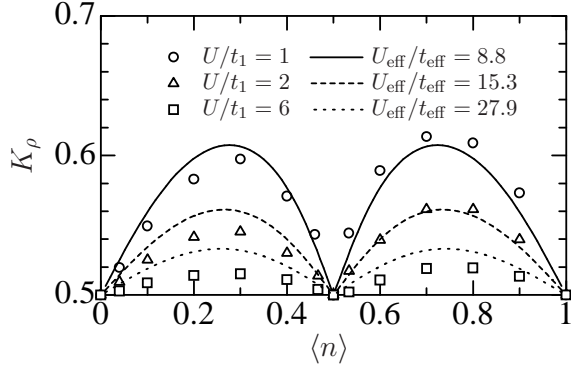


FIG. 4: Tomonaga–Luttinger parameter K_ρ from the DMRG approach for large dimerization, $t_2/t_1 = 0.1$, in comparison with the analytical result for the effective single-band Hubbard model. Recall that the band filling n of the dimerized Hubbard model corresponds to a filling $2n$ for the effective single-band Hubbard model.

2. Spin excitations

As our second quantity of interest we study the spin degrees of freedom at and around some commensurate band fillings. At half filling, $n = 1$, the dimerized Hubbard model is a band-Mott insulator for all $U/t_1 > 0$, and we expect a finite gap for spin excitations for all U/t_1 .

For small interaction strengths, the spin gap is of the order of the Peierls gap, $\Delta_s(U/t_1 \rightarrow 0) = \Delta_P = 2(t_1 - t_2)$. For large interactions, the spin degrees of freedom of the dimerized Hubbard model can be described by the one-dimensional Peierls–Hubbard model so that the spin gap to lowest order in t_1/U becomes

$$\Delta_s(t_1/U \rightarrow 0) \propto \frac{4t_1^2}{U} \left(\frac{t_1^2 - t_2^2}{t_1^2 + t_2^2} \right)^{2/3}, \quad (21)$$

in accordance with the results for the corresponding Peierls–Heisenberg model³⁰. Eq. (21) is applicable for $U/t_1 \gtrsim 4$. In the inset of Fig. 5 we show two examples for the finite-size scaling of the spin gap (3), $(t_2/t_1 = 0.5, U/t_1 = 10)$ and $(t_2/t_1 = 0.9, U/t_1 = 5)$. The dependence of the gap on the system size is quite small because in the ground state individual spin singlets are formed on the dimers so that the gapped spin excitations are rather localized in space.

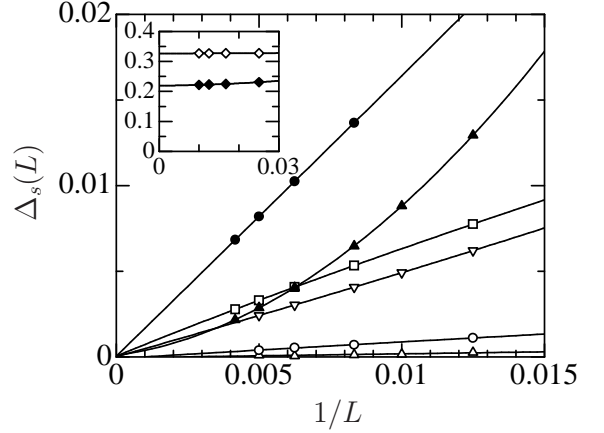


FIG. 5: Extrapolation of the spin gap $\Delta_s(L)$ of the dimerized Hubbard model. Solid symbols represent the results for weak dimerization ($t_2/t_1 = 0.9, U/t_1 = 5$) at infinitesimal doping of the band-Mott insulator ($n = 1$, triangles) and at small doping ($n = 0.95$, circles). Open symbols give the results for intermediate dimerization ($t_2/t_1 = 0.5, U/t_1 = 10$) at infinitesimal doping of the band-Mott insulator ($n = 1$, triangles), at the electron densities $n = 0.95$ (circles), $n = 0.8$ (squares), and at infinitesimal doping of the Mott–Hubbard insulator at quarter filling ($n = 0.5$, lower triangles). Inset: Extrapolation of the spin gap of the band-Mott insulator at half band-filling for $(t_2/t_1 = 0.9, U/t_1 = 5)$ (solid diamonds) and for $(t_2/t_1 = 0.5, U/t_1 = 10)$ (open diamonds).

It is more interesting to study the doping dependence of the spin gap. In Fig. 5 we plot $\Delta_s(L)$ as a function of system size for $(t_2/t_1 = 0.5, U/t_1 = 10)$ and for $(t_2/t_1 = 0.9, U/t_1 = 5)$ for several band fillings. As seen from the figure, the spin gap vanishes for all electron densities. In particular, at half band-filling it disappears as soon as the system is doped with an infinitesimal amount of holes. This can be understood in terms of the spin excitations of a half-filled system with two holes. Let us assume that the two holes are confined to a dimer.

Then, a spin excitations would remain the same local excitation as in the perfectly half-filled system which costs the finite energy (21). However, the holes are actually delocalized over the system because the breaking of two spin dimers cost twice Δ_s but the gain in kinetic energy is approximately

$$E_{it} \simeq 2(t_1 - t_2). \quad (22)$$

E_{it} is always larger than $2\Delta_s$. The mobile holes leave behind at least two broken spin dimers whose spin excitation energy vanishes in the thermodynamic limit.

Apparently, the dimerized Hubbard behaves differently from the two-leg Hubbard ladder at half band-filling where a spin-singlet pair is formed on each rung. The spin gap in the ladder system remains finite for finite hole doping. There the spin-singlet pairs themselves are mobile so that in the ground state an additional pair of holes is actually confined to a rung because the gain in kinetic energy due to the hole motion is smaller than the combined loss in the pairing energy and the kinetic energy of the spin dimers.

Finally, we investigate the spin gap for the quarter-filled dimerized Hubbard model at infinitesimal doping. In Fig. 5 we plot the size-dependence of the spin gap for the infinitesimally doped Mott–Hubbard insulator at quarter filling for ($t_2/t_1 = 0.5, U/t_1 = 10$). The extrapolated values are zero for all dimerization and interaction strengths. Therefore, the spin-gap liquid, suggested in the one-dimensional dimerized t - J model³¹ is not realized in the dimerized Hubbard model.

B. Dimerized extended Hubbard model

Now we turn to the case $V \neq 0$ in (1). We focus on the region around quarter filling where the nearest-neighbor interaction can lead to a CDW phase. This is known for the extended Hubbard model whose ground-state phase diagram was studied in detail recently^{14,19}.

1. Charge order

Previous studies^{32,33,34} suggested that the presence of a dimerization suppresses the CDW phase. Therefore, we investigate the dependence of the critical coupling V_c for the onset of the CDW. To this end we calculate the CDW order parameter χ from (5) as a function of the dimerization strength. For $V = 0$ we have $\chi = 0$ whereas, for large V , the CDW order parameter approaches its classical value, $\chi(V \rightarrow \infty) = 0.5$.

In Fig. 6 we show the order parameter $\chi(V)$ as a function of V/t_1 for dimerizations $t_2/t_1 = 1, 0.9, 0.5, 0.1$ for fixed $U/t_1 = 10$ at quarter band filling. In the absence of a Peierls modulation, $t_2/t_1 = 1$, i.e., in the extended single-band Hubbard model, $\chi(V)$ is finite above $V_c/t_1 \approx 2.65$, in agreement with previous work^{14,19,35}.

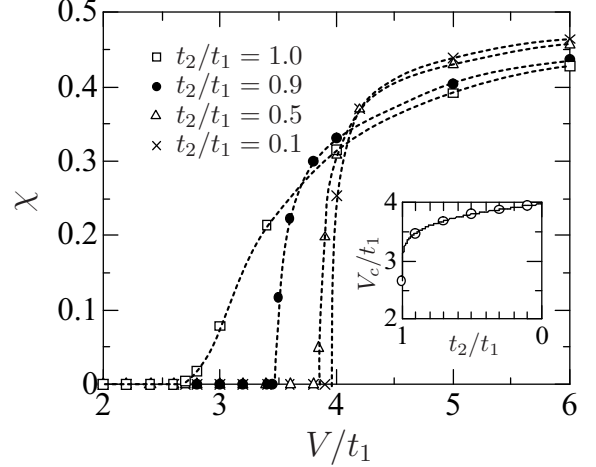


FIG. 6: CDW order parameter χ extrapolated to the thermodynamic limit $L \rightarrow \infty$ for $t_2/t_1 = 1, 0.9, 0.5$, and 0.1 with fixing $U/t_1 = 10$ at quarter filling. Lines are guides to the eyes. Inset: Estimated critical interaction strength V_c/t_1 for the CDW transition as a function of t_2/t_1 .

Apparently, the dimerization enhances the charge fluctuation on each dimer, and, consequently the tendency towards charge order is reduced.

In the presence of a dimerization the critical value for the onset of the CDW increases with increasing dimerization. Moreover, $\chi(V, t_2/t_1 < 1)$ rises up sharply above $V_c(t_2/t_1)$ even when t_2/t_1 is close to unity. We speculate that the transition remains continuous for all finite t_2/t_1 but the slope is infinite for all $t_2/t_1 > 0$. In the inset of Fig. 6 we show the critical value V_c/t_1 as a function of the dimerization strength t_2/t_1 . We find that V_c/t_1 changes rapidly for small t_2/t_1 and quickly saturates at its classical value for $t_2/t_1 = 0$. The value $V_c(t_2/t_1 = 0) = 4t_1$ is readily explained by considering an isolated dimer. In the isolated-dimer limit the energies of the Mott–Hubbard insulator and the CDW insulator are

$$E_0^{\text{MH}}/L = -t_1 + V_{\text{eff}} = -t_1 + V/4, \quad (23)$$

$$E_0^{\text{CDW}}/L = 0, \quad (24)$$

so that the criterion for the (discontinuous) transition is $E_0^{\text{MH}}(V_c) = E_0^{\text{CDW}}(V_c)$ which immediately gives $V_c/t_1 = 4$.

2. Tomonaga–Luttinger parameter

In the absence of a dimerization, the Tomonaga–Luttinger parameter decreases as a function of V/t_1 for fixed $U/t_1 > 4$ and reaches $K_\rho = 0.25$ at the critical coupling. When the CDW insulator is infinitesimally doped the system metalizes and $K_\rho^{\text{CDW}} = 1/8$ ^{19,29,36}.

For a finite dimerization, the quarter-filled system is a Mott–Hubbard insulator for small V/t_1 and finite U/t_1 . At infinitesimal doping we find $K_\rho^{\text{MH}}(V < V_c) = 1/2$ below the transition, independent of V . This is readily

understood from the fact that the effective model is the extended single-band Hubbard model at half band-filling for which the field-theoretical arguments for a density-driven Mott transition still apply. A qualitatively and quantitatively different behavior emerges from the transition to the CDW insulator at V_c . The Tomonaga-Luttinger parameter drops from $K_\rho = 1/2$ in the infinitesimally doped Mott-Hubbard insulator to $K_\rho < 1/8$, as we shall discuss in more detail now.

The dimerization has two prominent effects on K_ρ . First, it increases the strength of the Umklapp scattering which makes K_ρ smaller. Second, the dimerization suppresses the CDW instability which tends to make K_ρ larger. These effects are most apparent around quarter filling where the two tendencies compete with each other close to the CDW instability. Both effects increase upon decreasing t_2/t_1 . The first effect continues to develop progressively and leads to $U_{\text{eff}}/t_{\text{eff}} \rightarrow \infty$ as $t_2/t_1 \rightarrow 0$. As shown in Sect. III B 1, the second effect develops fast as a function of the dimerization and quickly saturates. Therefore, we expect that the first effect, a reduction of K_ρ upon dimerization, is more prominent but for quarter filling and in the vicinity of the transition to the CDW phase.

The reduction of K_ρ with dimerization can actually be inferred from the g -ology approach where the Tomonaga-Luttinger parameter near quarter filling is given by

$$K_\rho \approx \sqrt{\frac{2\pi v_F - V}{2\pi v_F + U + 5V}} \quad (25)$$

with $v_F = t_1 t_2 / \sqrt{t_1^2 + t_2^2}$. The formula shows that K_ρ decreases monotonously as a function of V and of t_2/t_1 . Naturally, g -ology cannot cover large dimerizations or the transition region where the increase of $K_\rho(V)$ upon dimerization becomes apparent.

In Fig. 7 we present the DMRG results for K_ρ as a function of V/t_1 at a hole doping and an electron doping of 5%, $\langle n \rangle = 0.5 \pm 0.025$, for $U/t_1 = 6$ and various dimerizations. The numerically exact DMRG results confirm the general expectations as expressed in the g -ology formula (25). The Tomonaga-Luttinger parameter decreases monotonously with V/t_1 for all dimerizations and, in general, it decreases as a function of t_2/t_1 for fixed V/t_1 . The fact that K_ρ is almost independent of t_2/t_1 for fixed $1 < V/t_1 < 2$ can be attributed to the above-mentioned competition between the Umklapp scattering and the charge ordering. For certain parameter regions, a change in the dimerization strength has almost no net effect on K_ρ because a change in the strength of the Umklapp scattering is compensated by a change in the mobility of the charge carriers. For the same parameter set $(V/t_1, t_2/t_1)$, K_ρ is generally somewhat smaller for the hole-doped case than for the electron-doped case but there is no difference in the qualitative behavior. This had to be expected because the system is particle-hole symmetric around quarter filling to lowest order in t_2/t_1 . From now on we shall focus on the case of hole doping.

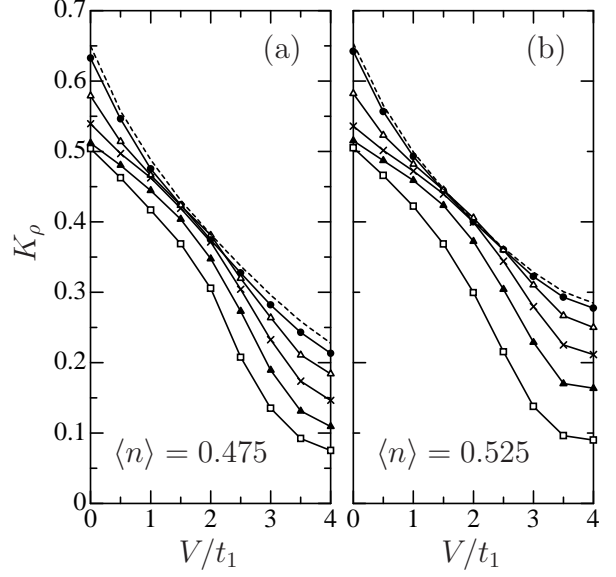


FIG. 7: Tomonaga-Luttinger parameter K_ρ in the dimerized extended Hubbard model as a function of the nearest-neighbor Coulomb interaction V/t_1 for $U/t_1 = 6$ and various dimerizations: $t_2/t_1 = 1$ (dashed line), $t_2/t_1 = 0.9$ (filled circles), $t_2/t_1 = 0.7$ (open triangles), $t_2/t_1 = 0.5$ (crosses), $t_2/t_1 = 0.3$ (filled triangles), and $t_2/t_1 = 0.1$ (open squares). The band filling is (a) $\langle n \rangle = 0.475$ and (b) $\langle n \rangle = 0.525$.

The Tomonaga-Luttinger parameter $K_\rho(V)$ changes most rapidly in the region $2 < V/t_1 < 4$ where the quarter-filled system undergoes the charge-ordering transition. For $V/t_1 \gtrsim 4$, we can interpret the system as a doped CDW insulator. In this region, we find that the dependence of K_ρ on the nearest-neighbor interaction V/t_1 is much weaker. This can be understood from the Taylor expansion of K_ρ for a slightly doped CDW insulator. Above the transition point ($V > V_c$) we generally expect¹⁹ that for $\delta = 1/2 - n \ll 1$ we have

$$K_\rho(t_2, U, V, 1/2 - \delta) = K_\rho^{\text{CDW}}(t_2, V) + \frac{\delta}{h(t_2, U, V)} + \dots, \quad (26)$$

where t_1 is used as energy unit. The prefactor $h(t_2, U, V)$ diverges exponentially at the critical interaction strength V_c but it rapidly tends to a constant for large V .

For infinitesimal doping, the Tomonaga-Luttinger parameter of the CDW insulator $K_\rho^{\text{CDW}}(t_2/t_1, V/t_1)$ also displays a smooth behavior as a function of V/t_1 and t_2/t_1 . In Fig. 8 we show $K_\rho^{\text{CDW}}(t_2/t_1, V/t_1)$ for $U = \infty$ and various dimerizations. As for the case of a finite doping we see that the dimerization tends to reduce the Tomonaga-Luttinger parameter. In the CDW phase this tendency is somewhat compensated by the influence of the nearest-neighbor Coulomb interaction which, for large interactions and for small doping of the CDW state, delocalizes the holes over the system and therefore increases the charge fluctuations which determine K_ρ via eq. (7).

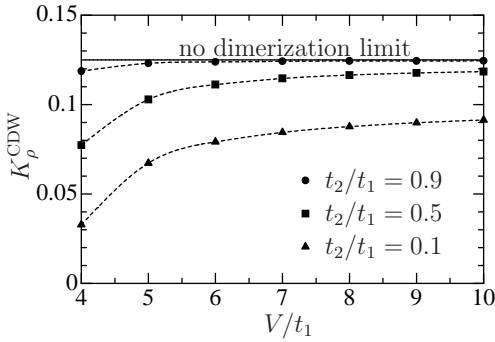


FIG. 8: Tomonaga–Luttinger parameter for the infinitesimally doped CDW insulator K_ρ^{CDW} as a function of V/t_1 for $t_2/t_1 = 0.9$, $t_2/t_1 = 0.5$, and $t_2/t_1 = 0.1$ at $U/t_1 = \infty$. The solid line corresponds to $K_\rho^{\text{CDW}} = 1/8$ when the dimerization is absent ($t_1 = t_2$), and the dotted lines are guides for the eyes.

The most important observation is the magnitude of the Tomonaga–Luttinger parameter for the doped insulators. For infinitesimal doping we find $K_\rho = 1/8$ in the absence of dimerization and even $K_\rho < 1/8$ in the presence of a dimerization. These small numbers persist for finite doping, as seen in Fig. 7. Therefore, depending on the choice of the dimerization and the nearest-neighbor Coulomb interaction, one can easily find parameter regions where $0.1 < K_\rho < 0.3$ can be realized for slightly doped quarter-filled chains.

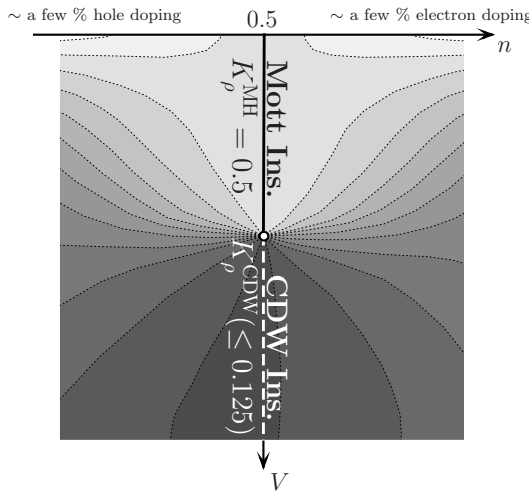


FIG. 9: Schematic phase diagram of the dimerized extended Hubbard model around quarter filling as a function of n and V . Variations of K_ρ are displayed by contour lines. Darker (brighter) color denotes smaller (larger) values of K_ρ .

Fig. 9 summarizes our findings for the Tomonaga–Luttinger parameter in a schematic phase diagram for the slightly doped quarter-filled dimerized extended Hubbard model. The Mott–Hubbard insulator (CDW insulator) can be characterized as $2k_F$ -SDW ($4k_F$ -CDW) states at quarter filling. Hence, the $2k_F$ -SDW and $4k_F$ -CDW cor-

relations are dominant for slightly doped Mott–Hubbard and CDW insulators, respectively, and their correlation functions decay algebraically with the asymptotical behavior $C^{2k_F\text{-SDW}}(r) \sim r^{-1-K_\rho}$ for Mott–Hubbard insulators and $C^{4k_F\text{-CDW}}(r) \sim r^{-4K_\rho}$ for CDW insulators. Thus, the value $K_\rho = 1/3$ discriminates the two types of (doped) insulators at finite doping. For an infinitesimally doped insulator we correctly find $K_\rho(V = V_{\text{dc}}) = 1/3$ for $V_{\text{dc}} = V_c$ but V_{dc} becomes actually smaller upon doping, as seen in Fig. 9.

C. Comparison with experiment

At last, we compare our theoretical result with experiments on $(\text{TMTTF})_2\text{X}$. The electron transfer matrix elements³⁷ are estimated to be $(t_1, t_2) = (137 \text{ meV}, 93 \text{ meV})$ for $\text{X} = \text{PF}_6^-$, $(t_1, t_2) = (140 \text{ meV}, 100 \text{ meV})$ for $\text{X} = \text{ClO}_4^-$, and $(t_1, t_2) = (133 \text{ meV}, 119 \text{ meV})$ for $\text{X} = \text{Br}$, i.e., $t_2/t_1 = 0.68, 0.71, 0.89$ for $\text{X} = \text{PF}_6^-, \text{ClO}_4^-, \text{Br}$, respectively. From the comparison with the optical gap^{38,39} the Coulomb parameters are estimated to be $U/t_1 \approx 7.0$ and $V/t_1 \approx 2.8$ for $(\text{TMTTF})_2\text{PF}_6^-$. A comparison with Fig. 7 and 9 shows that this parameter set leads to $K_\rho \approx 0.25$, in agreement with experimental estimates for the Tomonaga–Luttinger parameter from the temperature dependence of the resistivity^{6,40}. In view of the CDW state observed below $T \approx 100 \text{ K}$ ^{41,42,43}, the nearest-neighbor interaction could be even larger than $V/t_1 = 2.8$ which would further reduce K_ρ .

Unfortunately, such values for the nearest-neighbor interaction V/t_1 appear to contradict the results for the effective exchange interaction as deduced from the high-temperature data from the electron-spin-resonance (ESR) measurements⁴⁴, $J_{\text{exp}} = 420 \text{ K}, 430 \text{ K}, 500 \text{ K}$ for the anions $\text{X} = \text{PF}_6^-, \text{ClO}_4^-, \text{Br}$, respectively. In the presence of the dimerization and at quarter band-filling we can start from the effective extended single-band Hubbard model (12) and the spin degrees of freedom can be described in terms of the effective Heisenberg Hamiltonian (16). For $U/t_1 = 7.0$, the bare Hubbard model, $V = 0$ in (17), gives $J_{\text{eff}}(V = 0) = 499 \text{ K}, 564 \text{ K}, 841 \text{ K}$. The good agreement of the experimental and theoretical data for $V = 0$ implies that the nearest-neighbor interaction ought to be rather small. In particular, the a value $V = 2.8t_1$ for $(\text{TMTTF})_2\text{PF}_6^-$, leads to $J_{\text{eff}}(V = 2.8t_1) = 222 \text{ K}$, a factor of two smaller than the experimental estimate. Additinally, with small V to adjust J_{exp} , the resulting theoretical prediction for $K_\rho \approx 0.5$ from Fig. 7 is not compatible with the experimental estimate, $0.2 \lesssim K_\rho \lesssim 0.3$.

In order to reconcile this discrepancy we note that, in the ESR measurements, the curves are fitted to provide a good agreement with the Eggert–Affleck–Takahashi model⁴⁵ for the spin susceptibility of the $S = 1/2$ antiferromagnetic Heisenberg chain at elevated temperatures. However, substantial deviations occur for small temperatures, $T \lesssim 100 \text{ K}$. They could be the result

of a dimensional crossover⁴⁶ and the transition to the CDW phase. We are tempted to attribute the deviations to an effectively larger nearest-neighbor interaction at low temperatures. Recall that our electronic model is purely one-dimensional, and neither covers the influence of phonons^{47,48} nor does it give an account on the screening of the electron-electron interaction which may change drastically in the vicinity of the transition to the CDW state. Therefore, temperature may have a quite substantial influence on the value of the effective V -parameter in our model so that eq. (17) cannot be applied with the values for V/t_1 at $T = 0$ to explain the susceptibility data for $T > 100$ K.

In fact, in the CDW phase, the effective exchange interaction is given by $J_{\text{eff}}^{\text{CDW}}/t_1 \approx 4t_2^4/(2UV^2)$ which results in $J_{\text{eff}}^{\text{CDW}} = 14$ K if we use the parameters for $(\text{TMTTF})_2\text{PF}_6$. If the spin susceptibility could be measured in the (one-dimensional) CDW phase, the exchange interaction should be an order of magnitude smaller than in the high-temperature phase.

In $(\text{TMTSF})_2\text{PF}_6$, the hopping amplitudes are estimated as ($t_1 = 252$ meV, $t_2 = 209$ meV) and the effective Coulomb interactions are found to be weaker, $U/t_1 \sim 5$. Again, a weak nearest-neighbor Coulomb interaction, $V_1 \approx 0.5t_1$, would account for an exchange interaction $J_{\text{eff}} = 1.2 \cdot 10^3$ K which is compatible with the high-temperature experimental observation $J_{\text{exp}} \approx 1.4 \cdot 10^3$ K.

IV. SUMMARY

Using the DMRG method, we provided numerically exact results for the spin excitations, the CDW order parameter, and the Tomonaga–Luttinger parameter of the one-dimensional dimerized extended Hubbard model at and near commensurate fillings.

In the presence of a dimerization we confirm numerically that gap for the spin excitation is finite at half band-filling. However, the gap immediately disappears when the system is doped infinitesimally because there is no mechanism which confines the holes to a single dimer. This result is qualitatively consistent with a rapid suppression of the spin gap with Zn doping in the spin-Peierls Heisenberg system CuGeO_3 ⁴⁹, irrespective of the difficulty in metalization this material⁵⁰.

For the Tomonaga–Luttinger parameter the effects of the dimerization are weak in the absence of the nearest-neighbor Coulomb interaction V and away from quarter filling. At and near quarter filling, the lower Peierls band is essentially half filled and the dimerized Hubbard model at filling $n = 1/2 \pm \delta$ can be understood qualitatively and

even semi-quantitatively in terms of an effective single-band Hubbard model at electron density $2n$. From the result of the corresponding Hubbard model at half band-filling it immediately follows that $K_\rho = 1/2$ holds for the dimerized Hubbard model at infinitesimally doping away from quarter filling. Therefore, the Tomonaga–Luttinger parameter for the weakly doped quarter-filled system sensitively depends on the strength of the dimerization. In general, the dimerization tends to reduce K_ρ gradually because the effective scattering processes within the Peierls bands increase with the size of the Peierls gap.

In the presence of the nearest-neighbor Coulomb interaction, the case of quarter filling also deserves special attention because the Mott–Hubbard insulator goes over to a CDW insulator with a finite spin gap at a critical interaction strength V_c . The dimerization opposes the formation of the CDW phase, for example, the critical nearest-neighbor interaction shifts from $V_c/t_1 \approx 2.65$ in the absence of dimerization to $V_c/t_1 = 4$ in the dimer limit.

The suppression of the charge order at quarter filling by the dimerization is reflected in a tendency to stabilize the metallic state by the dimerization away from quarter band-filling. However, the increase of the electron-electron scattering by the nearest-neighbor Coulomb interaction overcomes that tendency and results in a net reduction of K_ρ as a function of the dimerization and the nearest-neighbor interaction, see Fig. 7. As a consequence, fairly small values, $K_\rho \approx 0.25$, can be obtained for a moderate five-percent doping of the quarter-filled dimerized extended Hubbard model at moderate Coulomb couplings, $U/t_1 = 6$, $V/t_1 = 3$.

It is difficult to reconcile all experimental data for the Bechgaard salts with our findings for the dimerized extended Hubbard model in one dimension. In order to find small values for the Tomonaga–Luttinger parameter, the Coulomb interactions must be large enough to reach the region of a (doped) CDW insulator which is not easily reconciled with the high-temperature data for the exchange interaction. We suspect that the one-dimensional dimerized extended Hubbard model is still too simplistic to describe the physics of the Bechgaard salts adequately.

Acknowledgments

We thank E. Jeckelmann for useful discussions. S.E. is supported by the Honjo International Scholarship Foundation.

¹ T. Ishiguro, K. Yamaji, and G. Saito, *Organic Superconductors* (Springer, Berlin, 1998).

² M. Lang and J. Müller, *The Physics of Superconductors, Vol. II*, ed. by K.-H. Bennemann and J.B. Ketterson (Springer, Berlin, 2003), p. 453.

³ V. Vescoli, L. Degiorgi, W. Henderson, G. Grüner, K.P.

Starkey, and L.K. Montgomery, *Science* **281**, 1181 (1998).
⁴ B. Dardel, D. Malterre, M. Grioni, P. Weibel, Y. Baer, J. Voit, and D. Jérôme, *Europhys. Lett.* **24**, 687 (1993).
⁵ F. Zwick, S. Brown, G. Margaritondo, C. Merlic, M. Onel-lion, J. Voit, and M. Grioni, *Phys. Rev. Lett.* **79**, 3982 (1997).
⁶ J. Moser, M. Gabay, P. Auban-Senzier, D. Jérôme, K. Bechgaard, and J.M. Fabre, *Eur. Phys. J. B* **1**, 39 (1998).
⁷ M. Dressel, A. Schwartz, G. Grüner, and L. Degiorgi, *Phys. Rev. Lett.* **77**, 398 (1996); A. Schwarz, M. Dressel, G. Grüner, V. Vescoli, L. Degiorgi, and T. Giamarchi, *Phys. Rev. B* **58**, 1261 (1998).
⁸ G. Mihály, I. Kézsmárki, F. Zámborszky, and L. Forró, *Phys. Rev. Lett.* **74**, 2670 (2000).
⁹ J. Moser, J.R. Cooper, D. Jérôme, B. Alavi, S.E. Brown, and K. Bechgaard, *Phys. Rev. Lett.* **84**, 2674 (2000).
¹⁰ C. Bourbonnais, *J. Phys. I (France)* **3**, 143 (1993).
¹¹ P. Wzietek, F. Creuzet, C. Bourbonnais, D. Jérôme, K. Bechgaard, and P. Batail, *J. Phys. I (France)* **3**, 171 (1993).
¹² T. Lorenz, M. Hofmann, M. Grüninger, A. Freimuth, G.S. Uhrig, M. Dumm, and M. Dressel, *Nature* **418**, 614 (2002).
¹³ S. Nishimoto, M. Takahashi, and Y. Ohta, *J. Phys. Soc. Jpn.* **69**, 1594 (2000).
¹⁴ F. Mila and X. Zotos, *Europhys. Lett.* **24**, 133 (1993).
¹⁵ K. Penc and F. Mila, *Phys. Rev. B* **50**, 11429 (1994).
¹⁶ M. Hase, I. Terasaki, and K. Uchinokura, *Phys. Rev. Lett.* **70**, 3651 (1993).
¹⁷ *Density-Matrix Renormalization*, ed. by I. Peschel, X. Wang, M. Kaulke, and K. Hallberg (Springer, Berlin, 1999).
¹⁸ U. Schollwöck, *Rev. Mod. Phys.* **77**, 259 (2005).
¹⁹ S. Ejima, F. Gebhard, and S. Nishimoto, *Europhys. Lett.* **70**, 492 (2005).
²⁰ H.J. Schulz, *Phys. Rev. Lett.* **64**, 2831 (1990).
²¹ H. Frahm and V.E. Korepin, *Phys. Rev. B* **42**, 10553 (1990).
²² M. Dzierzawa in *The Hubbard Model*, ed. by D. Baeriswyl, D.K. Campbell, J.M.P. Carmelo, F. Guinea, and E. Louis, NATO ASI Ser. B, Vol. **343** (Plenum Press, New York 1995), p. 327.
²³ R.M. Noack, S. Daul, and S. Kneer in Ref. [17], p. 197.
²⁴ S. Daul and R.M. Noack, *Phys. Rev. B* **58**, 2635 (1998).
²⁵ R.T. Clay, A.W. Sandvik, and D.K. Campbell, *Phys. Rev. B* **59**, 4665 (1999).
²⁶ J. Sólyom, *Adv. Phys.* **28**, 209 (1979).
²⁷ T. Giamarchi, *Quantum Physics in One Dimension* (Clarendon Press, Oxford, 2004).
²⁸ S. Andergassen, T. Enss, V. Meden, W. Metzner, U. Schollwöck, and K. Schönhammer, *Phys. Rev. B* **73**, 045125 (2006).
²⁹ T. Giamarchi, *Physica B* **230-232**, 975 (1997); T. Giamarchi and A.J. Millis, *Phys. Rev. B* **46**, 9325 (1992).
³⁰ J.W. Bray, L.V. Interrante, I.S. Jacobs, and J.C. Bonner, *The spin-Peierls transition* (Technical Information Series, New York, 1981).
³¹ S. Nishimoto and Y. Ohta, *Phys. Rev. B* **59**, 4738 (1999).
³² M. Tsuchiizu, H. Yoshioka, and Y. Suzumura, *J. Phys. Soc. Jpn.* **70**, 1460 (2001).
³³ Y. Shibata, S. Nishimoto, and Y. Ohta, *Phys. Rev. B* **64**, 235107 (2001).
³⁴ R.T. Clay, S. Mazumdar, and D.K. Campbell, *Phys. Rev. B* **67**, 115121 (2003).
³⁵ K. Sano and Y. Ōno, *Phys. Rev. B* **70**, 155102 (2004).
³⁶ H.J. Schulz in *Strongly Correlated Electronic Materials*, ed. by K.S. Bedell et al. (Addison-Wesley, Reading, 1994), p. 187.
³⁷ L. Ducasse, M. Abderrabba, J. Hoarau, M. Pesquer, B. Gallois, and J. Gaultier, *J. Phys. C* **19**, 3805 (1986); L. Ducasse, M. Abderrabba, B. Gallois, and D. Chasseau, *Synth. Met.* **19**, 327 (1987).
³⁸ F. Mila, *Phys. Rev. B* **52**, 4788 (1995).
³⁹ H. Benthien and E. Jeckelmann, *Eur. Phys. J. B* **44**, 287 (2005).
⁴⁰ B. Korin-Hamzić, E. Tafra, M. Basletić, A. Hamzić, and M. Dressel, *Phys. Rev. B* **73**, 115102 (2006).
⁴¹ F. Zamborszky, W. Yu, W. Raas, S.E. Brown, B. Alavi, C.A. Merlic, and A. Baur, *Phys. Rev. B* **66**, 081103(R) (2002).
⁴² F. Nad, P. Monceau, C. Carcel, and J.M. Fabre, *Phys. Rev. B* **62**, 1753 (2000).
⁴³ D.S. Chow, F. Zamborszky, B. Alavi, D.J. Tantillo, A. Baur, C.A. Merlic, and S.E. Brown, *Phys. Rev. Lett.* **89**, 1698 (2000).
⁴⁴ M. Dumm, A. Loidl, B.W. Fravel, K.P. Starkey, L.K. Montgomery, and M. Dressel, *Phys. Rev. B* **61**, 511 (2000); M. Dumm, A. Loidl, B. Alavi, K.P. Starkey, L.K. Montgomery, and M. Dressel, *Phys. Rev. B* **62**, 6512 (2000).
⁴⁵ S. Eggert, I. Affleck, and M. Takahashi, *Phys. Rev. Lett.* **73**, 332 (1994).
⁴⁶ M. Dressel, K. Petukhov, B. Salameh, P. Zornoza, and T. Giamarchi, *Phys. Rev. B* **71**, 075104 (2005).
⁴⁷ R.T. Clay and R.P. Hardikar, *Phys. Rev. Lett.* **95**, 096401 (2005).
⁴⁸ P. Maurel and M-B. Lepetit, *Phys. Rev. B* **62**, 10744 (2000).
⁴⁹ S.B. Oseroff, S-W. Cheong, B. Aktas, M.F. Hundley, Z. Fisk, and L.W. Rupp, Jr., *Phys. Rev. Lett.* **74**, 1450 (1995).
⁵⁰ I. Terasaki, R. Itti, N. Koshizuka, M. Hase, I. Tsukada, and K. Uchinokura, *Phys. Rev. B* **52**, 295 (1995).